Chapter 2
Borophenes: Insights and Predictions From Computational Analyses

Naiwrit Karmodak, Eluvathingal D. Jemmis, and Boris I. Yakobson

2.1 Introduction

Boron allotropes have attracted interest for decades, due to their exceptional properties and large number of applications [1–3]. However, the structural complexities and multicentered bonding patterns, in most of them, cause difficulties in understanding their structure-property relationships. The two-dimensional boron monoatomic layers discovered recently on metal templates are no exception to this [4, 5]. Though most of these planar boron phases are not composed of any polyhedral fragments as that of three-dimensional allotropes, the structural controversies and possibilities of multiple polymorphs [6, 7] remind one of the early histories of 3D boron allotropes. Depending upon the crystallization techniques and the growth temperatures, the 3D boron allotropes are seen to form structures with varying number of atoms and unit cell symmetry [1–3, 8, 9]. Stability of those forms also notably varies. For the two-dimensional phases, on the other hand, slight changes in the choice of boron deposition rate, the nature of the substrate, and its temperature introduce dramatic variations in the structure [4, 5, 10–13]. This is not an artifact of experimental uncertainties, with now several laboratories around the world attempting such experiments. Is there an inherent reason for this variability?

N. Karmodak
Department of Physics, University of North Texas, Denton, TX, USA

E. D. Jemmis (✉)
IPC Department, Indian Institute of Science, Bangalore, Karnataka, India
e-mail: jemmis@iisc.ac.in

B. I. Yakobson (✉)
Department of Materials Science and NanoEngineering and Department of Chemistry, Rice University, Houston, TX, USA
e-mail: biy@rice.edu

I. Matsuda, K. Wu (eds.), *2D Boron: Boraphene, Borophene, Boronene*,
https://doi.org/10.1007/978-3-030-49999-0_2

Much before the experimental reports, several theoretical studies attempted to understand the structural possibilities of the borophene phases [14–22]. Since the discovery of graphene, the common approach to achieve the two-dimensional phases has been starting from smaller precursors and then extending along in two dimensions or exfoliating the bulk layered allotropes into its two-dimensional counterparts. However, many fragments of the three-dimensional boron allotropes are unstable in the isolated form. Moreover, apart from the polyhedral boranes, planar precursors are not known, which could be related as suitable structural motifs resulting into the borophene phases upon extension. Thus, the search for alternatives yielded some initial ideas of the structural possibilities of 2D boron. Inspired by the resemblance in chemistry of boron and carbon [23], several attempts were made to construct boron nanostructures based on the frameworks of carbon compounds. This leads to the emergence of a large number of boron structures different from the 3D boron allotropes with varying structural possibilities and properties [6, 7, 14, 24].

In this chapter, we focus on the attempts made to understand the chemistry and physics of two-dimensional boron allotropes, overviewing the theoretical works on the structural variety and stability of the different borophene phases. The discussion begins with the studies made prior to the synthesis of these phases on metals, which includes the chemistry of smaller boron clusters and the different strategies proposed to extend those clusters to 2D boron phases. This is followed by an analysis of the forces, regulating and controlling the stability and geometry of boron sheets. The structural possibilities of the recently synthesized borophene phases on metal templates are then reviewed. Finally, we summarize with a growth mechanism of the 2D phases on the metal templates focusing on the different experimental conditions, such as growth temperature, choice of boron sources, and reactivity of the metal surfaces, that play significant role in bringing the structural variations of the boron sheets.

2.2 2D Boron Clusters, Borophene's Conceptual Ancestors

Following the connection between benzenoid aromaticity and polyhedral boranes [23], several 2D boron clusters have been predicted. The idea of obtaining most probable geometries for B_n, where n varies through different values, is that with higher values of n probable structures of 2D boron phases would be obtained [14, 24, 25]. Structural preferences of aromatic hydrocarbons are often altered by addition or removal of electrons [26, 27]. This is a familiar situation known for benzene (C_6H_6) and cyclopentadienyl anion ($C_5H_5^-$), where removal of two electrons from the valence shell transforms the planar geometries into pentagonal pyramid and square pyramid structures for $C_6H_6^{+2}$ and $C_5H_5^+$, respectively. In the polyhedral boranes, each boron atom contributes two of its valence electrons toward skeletal bonding and one electron is used for exohedral B-H bond formation. Thus, based on the idea that the removal of H atoms from the polyhedral boranes would provide excess electrons and favor similar structural transformations to planar forms, attempts for stabilizing

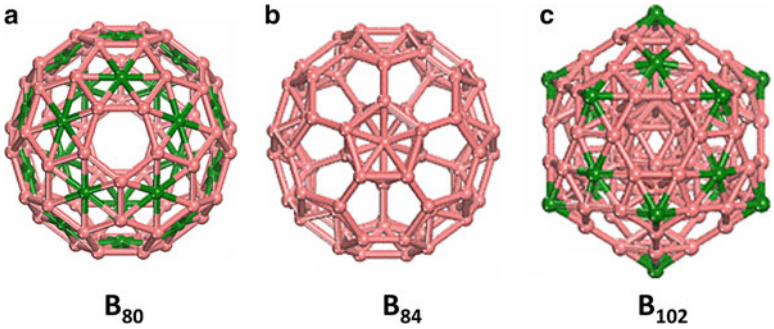

Fig. 2.1 The hollow and stuffed boron fullerenes reprinted from ref. [36] (**a**) The B_{80} cluster obtained from B_{60} by adding twenty more B atoms at the hexagonal center. (**b**) B_{84} fragment of β-boron allotrope. (**c**) The B_{102} fullerene obtained from the B_{84} by adding the 18 extra B atoms, to satisfy the required number of electrons, upon separating the fragment from the 3D unit cell

the boron clusters without the attached H atoms initiated [28–32]. A systematic theoretical study by Boustani et al. reported a number of such boron clusters for the first time [14, 24, 25]. The geometries are formed of triangular networks of boron atoms. Most of the clusters prefer a cyclic quasi-planar arrangement, with the peripheral boron rings attached with one or more number of boron atoms in the center.

Meanwhile, a stable cage cluster with 80 boron atoms, starting from the structure of C_{60} Buckminster fullerene, was predicted as the prototype for the boron fullerenes by Yakobson et al. (shown in Fig. 2.1a) [33–35]. A simple substitution of all the C atoms in C_{60} with B atoms would result in a B_{60} cluster, electron-deficient and unstable. The required 60 electrons could be provided by addition of 20 more boron atoms at the centers of the 20 hexagonal rings (green spheres in Fig. 2.1a), such that each boron atom would give its three valence electrons toward the skeletal bonding. This yields a total 80 boron atoms cluster, composed of pentagonal and triangular rings. Though a theoretical study later by Jemmis and coworkers showed that the stability of such fullerene is further enhanced by stuffing an icosahedral B_{12} unit inside the boron cage-spheres (Fig. 2.1b–c) [36, 37], the B_{80} structure was indeed the first demonstration that boron nanostructures with only triangular rings could not be stable, while a more complex pattern can.

In order to reveal the entire structural spectrum of the boron clusters with varying sizes, several experimental techniques have been developed [38–40]. A laser ablation method designed by Wang et al. and the accompanying theoretical structure search methods provide a detailed understanding of the geometries and electronic structures of these clusters [7, 41, 42], Figure 2.2 shows the structural variations in the boron clusters as the size increases. The planar clusters are obtained as the most stable isomers only up to 19 boron atoms. Above this, the cage isomers have competitive stability with respect to the planar structures. Most of these clusters also show the emergence of boron rings (denoted as holes) with greater than three

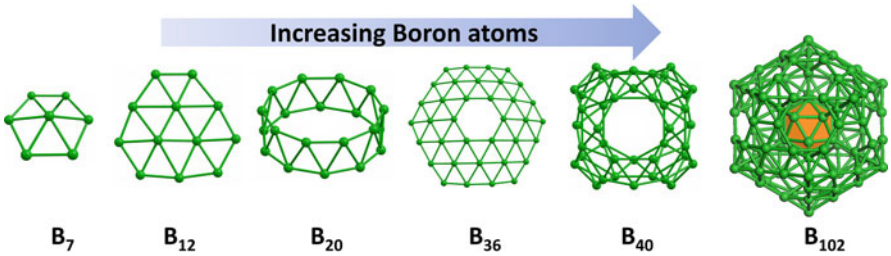

Fig. 2.2 The structural variations of the boron clusters with the increasing number of B atoms

boron atoms [7]. The structural transformations to tubular clusters are seen starting from 20 atoms and eventually become a near-spherical cluster with around 30 to 40 boron atoms [43]. The near-spherical clusters preferred stuffing with I_h-B_{12} from around a hundred or more number of boron atoms. Wang et al. introduced the term borospherenes for spherical clusters [44, 45], and from the planar cluster with a hole also the term *borophene* [46], similar to already used name *boraphene* for monoatomic boron layer in earlier Japanese study [47]. The B_{36} cluster is composed of a hexagonal ring of boron atoms in the center surrounded by 48 triangular rings. Though the search for larger boron clusters does not always lead to planar geometries, it makes it more evident that indeed the holes-vacancies are essential [16, 22, 33] for the stability of boron nanosheets. Besides, the 2D expansion of planar clusters parallels the shape of things in the realm of 2D boron allotropes. The interplay between holes (rings larger than three-membered that is atomic vacancies in the triangular lattice [22]) and the stability of 2D boron polymorphs is discussed next.

2.3 The Structural Possibilities of Borophene Phases

The structural identity of the borophene phase is subtle and has undergone several revisions since its conception decades back. Based on the structural patterns of the planar clusters, a triangular planar sheet was proposed initially out of the graphitic boron layers present in several metal diborides, especially the MgB_2 (Fig. 2.3a–c) [48]. Here, Mg atoms occupy the central positions to each hexagon (Fig. 2.3b), above and below the boron layers. With one electron less than carbon, the hexagonal unit cell with two boron atoms has a deficiency of two electrons. The electron requirement is satisfied by the charge transfer of electrons from the metal atoms, such that Mg gets a formal di-positive charge, whereas the boron becomes negative B^-. An electron added to the boron valence shell makes it isoelectronic to graphene, resulting in a stoichiometric formula $Mg^{+2}(B^-)_2$. Therefore, in order to stabilize these boron layers without any metal and obtain an all-boron sheet, it was thought that the substitution of Mg by boron would also satisfy the electron count [49, 50].

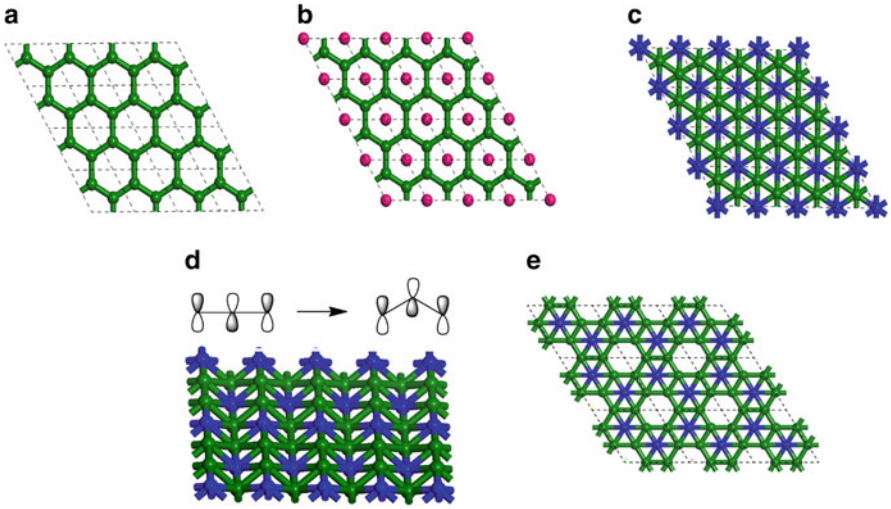

Fig. 2.3 A diagram showing the relationship between graphene and borophene. (**a**) Graphitic sheet of boron. (**b**) MgB_2 layer. (**c**) The planar triangular sheet of boron obtained from MgB_2 by substitution of Mg by B atoms. (**d**) The buckled triangular sheet and the nonplanar rearrangement of boron atoms reducing the antibonding overlap. (**e**) The α-boron sheet. (Reproduced from ref. [51])

The addition of the boron atoms introduces several differences relative to MgB_2. Firstly, the added boron atoms at the center remain in the same plane as that of the other boron atoms of the hexagonal layer, resulting in the planar triangular sheet with unit cell formula of B-B_2 (Fig. 2.3c). On the other hand, with the addition of each extra boron atom, three electrons are brought into the skeletal bonding instead of two electrons as needed per unit cell. These excess electrons would certainly occupy the antibonding bands, leading to destabilization of the sheet. The stability of the boron sheet is found to increase by an out-of-plane rearrangement of the boron atoms, since the antibonding interaction of the frontier bands is reduced [51–53]. A qualitative representation of the frontier *p* bands due to the nonplanar arrangement of the boron atoms is shown in Fig. 2.3d. Corresponding quasi-planar all-triangular sheet is also obtained from B_7 cluster following the Aufbau principle as proposed by Boustani et al. (Fig. 2.4) [24]. The hexagonal pyramid B_7 unit could extend to the curved surfaces of the fullerenes (borospherenes) and nanotubes, when the adjacent apices of the two hexagonal pyramids joined with one another by sharing a B-B bond are pointed in the same direction (pathway a in Fig. 2.4). An alternating arrangement of the apices leads to the formation of triangulated quasi-planar sheet (pathway b in Fig. 2.4).

Further, the Aufbau pyramids are quite conspicuous in cage cluster B_{80}, which also displays B-vacant pentagonal sites [33, 35], importantly suggesting that its unfolded planar form would also require a portion of B-vacant hexagons. Indeed, on the heels of this cluster proposal, Tang and Ismail-Beigi realized that in comparison

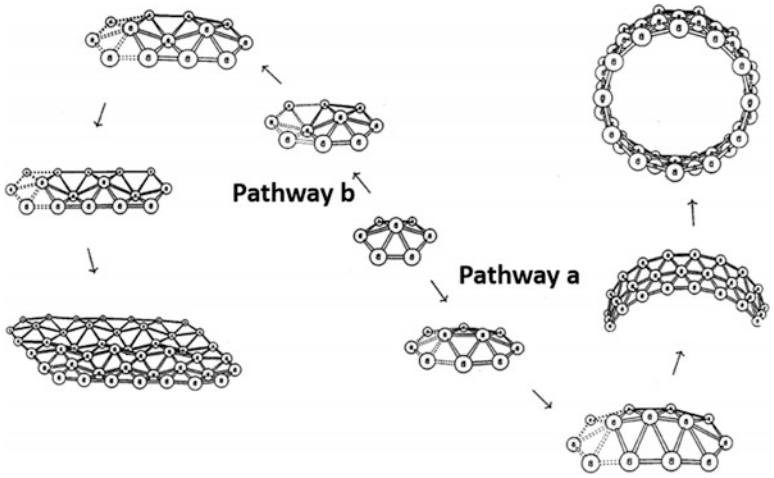

Fig. 2.4 The Aufbau principle as proposed by Boustani et al. [24]. for constructing extended boron nanostructures starting from the smaller B_7 hexagonal bipyramid cluster. The pathway a denotes the possible route to obtain the tubular structures, whereas pathway b corresponds to the quasi-planar boron sheet. (Reprinted from ref. [24] Reprinted by permission from I. Boustani, Systematic ab initio investigation of bare boron clusters: Determination of the geometry and electronic structures of B_n ($n = 2$–14), Phys. Rev. B 55, 16,426 (1997). Copyright (1997) by the American Physical Society)

to the buckling, the planar triangular sheet is better stabilized by the formation of hexagonal holes [16]. The planar triangular sheet (B-B_2) has one excess electron in each unit cell of three boron atoms. Therefore, the removal of one-thirds of the boron atoms per unit cell would reduce the excess electron density and result an electron count similar to graphene or the MgB_2 [42, 51]. In general, this could be achieved by the removal of one boron atom from every supercell of nine boron atoms (B-B_2)$_3$ (or B_3-B_6), denoted as the α-boron sheet [16]. The sheet thus obtained would be isomorphic to the unfolded B_{80} fullerene structure [33, 35]. The significance of holes becomes obvious and gives rise to the concept of the hexagonal hole density (*HD*), which is defined as [16]:

$$Hole\ density(HD) = \frac{number\ of\ hexagonal\ holes}{total\ boron\ atoms\ in\ the\ original\ triangular\ sheet\ without\ holes}$$

The triangular planar and buckled boron sheets would have $HD = 0$, whereas the α-boron sheet should have $HD = 1/9$. A number of 2D boron phases are obtained by varying the number of hexagonal holes and their arrangements within the unit cell [17, 18, 22]. The structural search methods such as cluster expansion (CE) and particle swarm optimization (PSO) are employed to reveal all possibilities of

boron phases with different unit cell formula and HD. The boron sheet is assumed to be a pseudo-alloy composed of boron atoms and hexagonal holes, denoted as $B_{1-\nu}[]_\nu$ [19]. Here ν is the hexagonal hole (vacancy, v) density, which is varied through different values to get the optimum choice. The binding energies per atom are calculated using the first-principles approach to compare the stability of these boron sheets. Though highest stability is obtained for the sheets with HD around 1/9, several structural polymorphs are seen for each hole density distribution [19, 22]. A number of semantic classifications are made to name these phases based on the hexagonal HD per unit cell, the coordination numbers of the B atoms, and the structural arrangements. Figure 2.5 shows the structural possibilities of a few boron sheets with varying HD; the corresponding relative stabilities in vacuum, with respect to α-boron sheet, calculated using density functional theory (DFT) are given in Table 2.1, also providing the different names used in the literature to denote these sheets. Among the different nomenclatures, the one proposed based on the connectivity of the boron atoms by Wu. et al. is used more often to denote the borophene phases [17]. In the discussion here, we follow this nomenclature. As per this classification, the monolayer phases are denoted with Greek alphabets such as α, β, and so on, representing the different coordination numbers (CN) of the boron atoms, followed by arbitrary roman numerals as the subscript. The sheets with coordination numbers (CN) of 5 and 6 are named as the α-phases. The β-sheets are those having CN varying from 4 to 6, whereas the sheets with CN = 4 and 5 constitute the χ-type. The ψ-type are the sheets with CN = 3, 4 and 5. The sheets

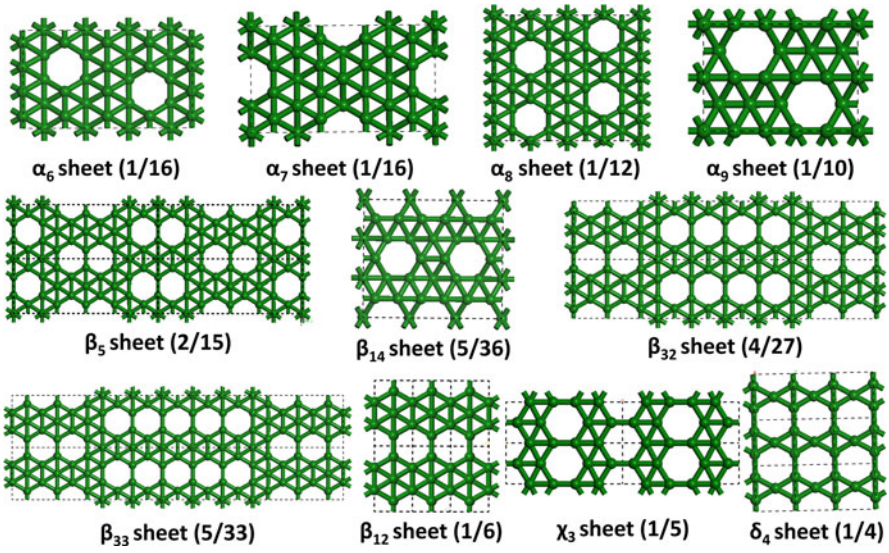

Fig. 2.5 The monolayer borophene phases with varying holes densities, HD. The boron phases are denoted using the nomenclature of Wu el. al [17]. The HD values are given within the parenthesis. (Reproduced from ref. [51])

Table 2.1 The relative binding energy (BE) of the monolayer borophene phases in meV/atom with different HD, calculated using DFT-PBE functional. The BE is reported with respect to α-boron sheet

Sheet	Notations in literature	HD	BE
δ_6'	Flat triangular sheet [16],	0	312
δ_6	δ_6 [17], buckled triangular sheet [16], Ψ_2 [54], B_Δ [55]	0	96
α_6	1/16 sheet [56]	1/16 (0.062)	82
α_7	1/16 sheet [56]	1/16 (0.062)	90
α_8	–	1/12 (0.083)	59
α_9	–	1/10 (0.100)	32
α	α′ [17], struc-1/9 [18], α [16]	1/9 (0.111)	0
β_5	$\nu_{2/15}$ [19], $g_{2/15}$ [22], β_5 [17], 2/15 sheet [18], β_3 [54]	2/15 (0.133)	1
β_{14}	5/36 sheet [56]	5/36 (0.139)	59
β_{32}	–	4/27 (0.148)	50
β_{33}	–	5/33 (0.151)	28
β_{12}	β_{12} [5, 17], struc-h [18], $\nu_{1/6}$ [16], β_5 [54],B ▫ [55]	1/6 (0.167)	54
χ_3	$\chi\diamond_3$ [5, 17], struc-1/5 [18], χ_1 [54], B [55]	1/5 (0.200)	43
δ_4	δ_4 [17]	1/4 (0.250)	313
δ_3	$\delta\bigcirc_3$ [17], Ψ_1 [54], hexagonal [16], B [55]	1/3 (0.333)	900

with the single value of the CN are named as δ-types; however, the subscripts in this case denote the value of the CN number. Therefore, the planar and the buckled triangular sheets are given the names δ_6 and δ_6', respectively, since each boron atom is connected to six other boron atoms, whereas the graphitic boron sheet is denoted as δ_3 phase.

2.4 Borophene Phases on Metal Substrates

The metal substrate-template introduces significant effects determining the stability of two-dimensional boron phases, in addition to the hexagonal hole density and out-of-plane buckling. The overlap with the metal bands would indeed cause electron transfer to the boron sheet. Therefore, one can assume initially that the sheets with higher electron deficiency should have improved stability on metal surfaces. This is also seen in a theoretical study by Zhang et al., where hexagonal boron sheet (δ_3) shows greater stability compared to both the planar triangular (δ_6) and α-sheet on metal surfaces, such as Mg(0001), Al(111), Ti(0001), Au(111), and Ag(111) [57]. However, later on Yakobson and coworkers found that for each metal surface, the stability would vary drastically depending upon the HD of the sheets and the experimental conditions [15, 20, 21]. Based upon the binding energies of the sheets, the metal surfaces are classified into two types. The first type consists of the metal diborides, such as MgB_2 and TiB_2, which are found to serve as the promising materials, where the boron terminated surface could provide boron phases

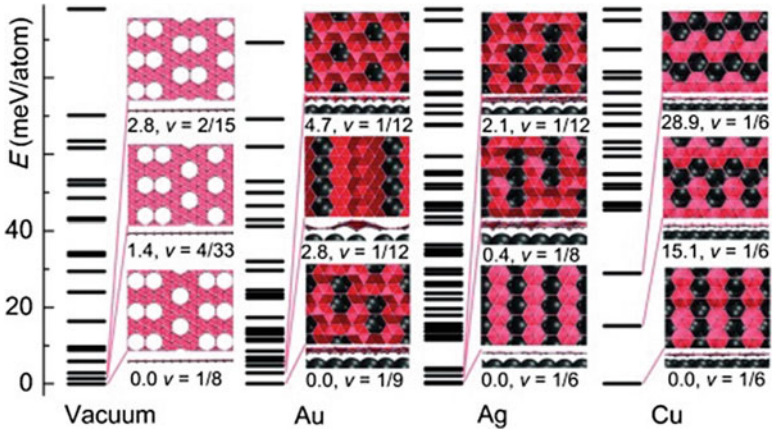

Fig. 2.6 The energy spectrum of isolated borophene phases and in the presence of Cu, Ag and Au surfaces as a function of the HD, taken from Ref. [19]. Here ν denotes the HD and the structures of the three most stable phases are shown within the insets

upon its saturation with boron atoms or evaporation of the metal atoms present underneath the surface boron layers. By tuning the experimental conditions, such as the temperature or the pressure, or even gate voltage applied to the substrate, structural preferences of the boron sheets could be varied to large extent [15, 20, 21].

On the other hand, the metal surfaces, i.e., Cu, and noble Ag and Au comprise the second category, which are suggested as the preferable substrate for the chemical vapor deposition growth of boron sheets [15, 20, 21]. Employing the structural search algorithms, the most probable polymorph of the borophene phases for each of these metal templates is determined [19]. Figure 2.6 shows the relative stability for different borophene phases with varying HD in the presence of the metal surfaces. Compared to the isolated sheets, the β_{12} sheet with 1/6 HD has the maximum stability on Cu surface, whereas the Ag surface shows preferences for several sheets with varying HD. The binding energy remains similar for a range of HD near 1/6. The Au surface has similar stability patterns as obtained for the isolated sheets. Though the sheet with 1/9 HD has the maximum stability, the relative differences in the binding energies for the other sheets are reduced compared to the values without the metal templates.

The structural possibilities of boron phases on metal templates are largely dependent upon the surface energies and work function values of the metal atoms [19, 58]. The surface energies determine whether the adsorbed boron atoms would form metal-boron alloys or proceed to the synthesis of extended 2D sheets, whereas the charge transfer possibility from the metal surfaces to the synthesized boron sheets is governed by the corresponding work function values. Having the highest surface energy, the Cu(111) surface prefers the sheets with higher HD. Though for both the Ag(111) and Au(111) surfaces, the surface energies are slightly lower, the

lower work function values preferentially stabilizes the electron-deficient sheets on Ag(111) surface as well. On the other hand, the reactivity for Au(111) surface is lowest because of having lower surface energy values and higher work function. Hence, the stability trend of the boron sheets remains unchanged as for the isolated sheets. Moreover, in order to enhance the interaction with the metal substrates, the sheets undergo considerable buckling from the planarity [59].

2.5 Experimental Synthesis of Borophene

Influenced by the previous theoretical studies [15] and knowledge available from the synthetic procedures for the other elemental two-dimensional phases, the first-ever approach to synthesize monoatomic 2D boron polymorph was reported on Ag(111) surface. The two different groups succeeded in synthesizing monolayer boron phases by vapor phase deposition of boron atoms under ultrahigh vacuum (UHV) conditions. Based on the in situ scanning tunneling microscopy (STM) images, two phases are detected in one of the studies by Mannix et al. [4], denoted as striped and homogeneous phase (Fig. 2.7a–b). The lower growth temperature and higher deposition rate favor the formation of homogeneous phase, whereas with slightly higher temperature and lower deposition rate stripped phase is synthesized. The other report is by Feng et al., where the formation of two boron sheets are also reported, denoted as the S1 and S2 phases (Fig. 2.7c–d) [5]. At a temperature of around 570 K, the S1 phase is obtained, while S2 phase appears by annealing the metal template to 650 K. The STM images of both sheets show great resemblance to the phases obtained by Mannix et al. (Fig. 2.7a–d), but the structures proposed were different. The incoherence in the borophene structure interpretation eventually attracted several repeating experiments and characterizations. However, every experiment results into different consequences (Fig. 2.7e–f), such that either intermixed phases containing both the S1 and S2 phase domains are obtained [60] or completely new phases appeared [11]. This observation is generally in tune with the theory, predicting a number of 2D boron polymorphs to be formed on Ag surfaces with very similar binding energies [19, 22]

Apart from the growth temperature and the deposition rate, the structural possibilities of boron phases vary, depending upon the template surface. The deposition of boron atoms on Al (111) surface influences a honeycomb lattice structure, similar to graphene (Fig. 2.8a) [61]. On the other hand, the boron sheets formed on the Au (111) surface prefer a herringbone pattern as shown in Fig. 2.8b [10]. Two-dimensional phases are also obtained on Cu surfaces. The vapor deposition of a mixture of pure boron and boron oxide mixtures in the presence of hydrogen gas as the reducing agent led to the formation of icosahedral sheets with a thickness of around 0.8 nm^{12}, whereas monolayer phases are formed when only boron vapors are used at 770 K with a deposition rate of 0.05 monolayer area per minute (ML min^{-1}) [13]. The growth kinetics and the sizes of the boron sheets varied to great extent on Cu template, compared to both Ag and Au surfaces (Fig. 2.8c).

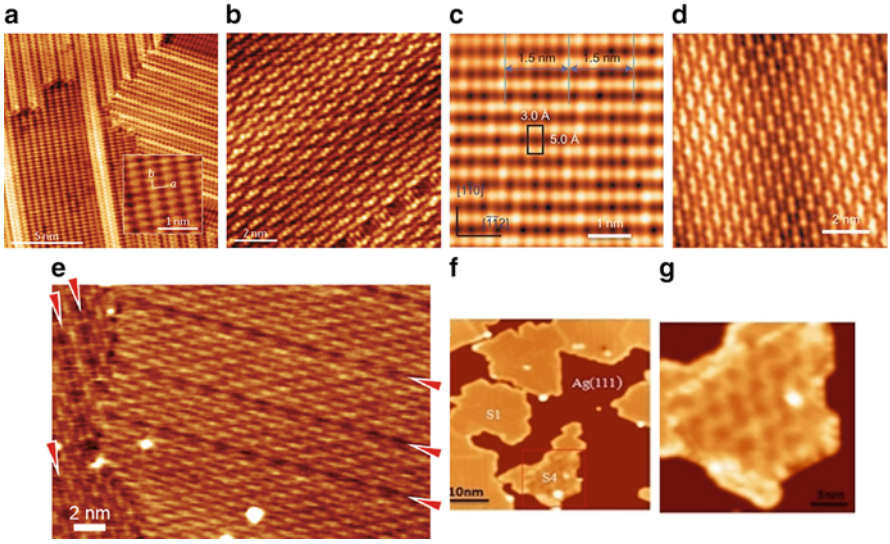

Fig. 2.7 The experimental STM images of the borophene phases obtained on Ag(111) surface reproduced from ref. [4, 5, 11]. (**a**) and (**b**) The stripped and the homogeneous phase reported by Mannix et al [4]. (Reprinted by permission from A. J. Mannix et al., Science 350, 1513 (2015). Copyright (2015) American Association for the Advancement of Science. (**c**) and (**d**) The S1 and S2 borophene phases reported in ref. by Feng et al [5]. (By courtesy of Kehui Wu). (**e**) The intermixed phase from S1 and S2 phases obtained by Liu et al. The red arrows denoted the separating regions between the two phases. (**f**) and (**g**) The formation of S4 phase along with the S1 phase reported in Ref. [11] (By courtesy of Kehui Wu)

The structural models of synthesized borophene phases on metal templates include the following.

2.5.1 Borophene Phase on Ag(111) Surface

S1 Phase and the Striped Phase The structural models proposed for the S1 and stripped borophene phases brought in some stimulating controversy. The STM images for both the stripped phase and S1 phase contains parallel arrangement of lighter and darker protrusions, with periodicities of 3 Å along the rows and 5 Å across the rows (Fig. 2.6a–b) [4, 5]. The linear arrangement of the lighter protrusions corresponds to the electron-rich regions, whereas the darker protrusion denotes the region with electron deficiency. The S1 phase is predicted to match with the β_{12} boron sheet with the HD of 1/6, whereas the stripped phase was correlated to the buckled triangular sheet with zero HD (denoted as δ_6' sheet). However, in later theoretical and experimental studies, it has been seen that both the phases are similar, pointing to the β_{12} boron sheet (Fig. 2.9a) [51, 54, 62], which has been

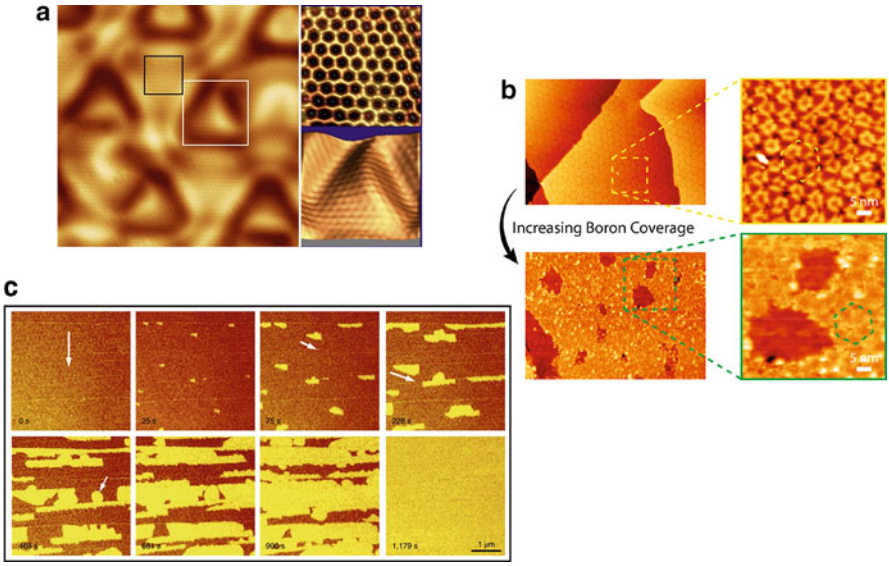

Fig. 2.8 (**a**) The hexagonal boron phase obtained on Al (111) surface [61]. (By courtesy of Kehui Wu). (**b**) The herringbone arrangement of the smaller boron islands formed by the deposition of boron atoms on Au (111) surface [10]. The smaller islands form the extended phases with higher boron coverage. (**c**) The monoatomic boron phases formed on Cu(111) surface at different time period [13]. (Reprinted from ref. [10, 13, 61] (By courtesy of A. Gozar))

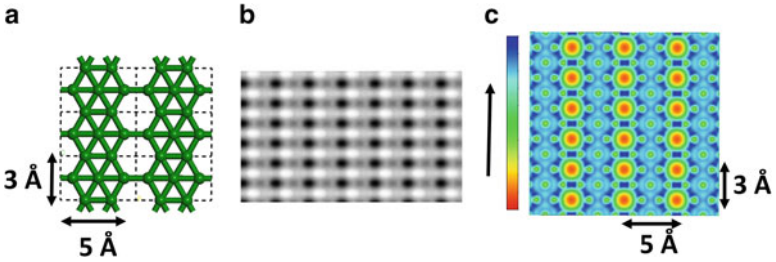

Fig. 2.9 The structure (**a**), simulated STM image (**b**), and the electron density distribution plot of β_{12} sheet (**c**). (Reproduced from ref. [51])

pointed out earlier theoretically as the most favorable phase on the Ag(111) surface by Zhang et al. [19]. The simulated STM images for the β_{12} boron sheet is shown in Fig. 2.9. The filled and vacant (holes) hexagonal units, arranged in linear fashion for β_{12} sheet, give rise to the linear patterns of lighter and darker protrusions in the simulated STM image (Fig. 2.9b–c). The filled hexagons in the β_{12} sheet have the lateral length of 3 Å, whereas the longitudinal length is around 5 Å.

S2 Borophene Phase and the Homogeneous Phase on Ag(111) Surface The S2 borophene phase has a brick-wall-type arrangement of the electron-rich and -

deficient regions, as the STM images (Fig. 2.7d) show alternate patterns for the lighter and darker protrusions [5]. Though much detailed information is not obtained for the homogeneous phase, STM image shows a similar pattern as the S2 phase, shown in Fig. 2.7b [4]. The χ_3 sheet with HD of 1/5 is initially predicted to be the precise structure for the S2 phase, despite periodicities have slight disagreement with the experimental values. The interrow periodicity is around 8.41 Å, and along the rows, it is 2.99 Å for χ_3 sheet, while the corresponding experimental values are around 15 Å and 4.3 Å, respectively. However, S2 phase could have multiple structural possibilities, depending upon its growth conditions [51].

The transformation of the S1 phase to S2 phase has been observed during the experiment upon increase in temperature [5]. This rearrangement is to readjust the electron requirement due to nonplanar undulations in the sheets with enhancement of temperature [59]. The overlap between the β_{12} sheet and the Ag surface would vary from one surface region to the other, depending upon the arrangement of the boron and the surface metal atoms. For the regions where the overlap would be greater, the HD of the sheet would increase further from 1/6 such that the greater charge transfer from the metal surface could be accommodated. On the other hand, the HD would reduce for those regions of the sheet where the connectivity between the sheet and the metal surface gets reduced. The χ_3 sheet with HD of 1/5 is one of the possibilities for the phases with enhanced HD. The other possibilities could be the β (β_5, $\beta_{32}$and β_{33}) sheets with slightly lower HD and formed of alternating filled and vacant hexagons as shown in Fig. 2.10. The relative stability of these sheets on Ag surface is slightly less compared to χ_3 sheet. Alternating filled and vacant hexagonal patterns would form a brick-wall-type arrangement for the lighter and darker protrusions in the corresponding simulated STM images (Fig. 2.10). The periodicities of β_5 sheet is 14.62 Å and 5.06 Å along and across the rows, respectively, which are almost similar as obtained for the S2 phase. The other two β-sheets have slightly higher periodic length along the rows; however, the arrangement across the rows coincides with the S2 phase.

2.5.2 Borophene Phases Synthesized on Cu Surface

The structural possibilities of 2D boron phases on Cu surface are largely dependent upon choice of boron sources as also evident from the recent synthetic reports [12, 13]. The boron nanostructures formed from deposition of boron oxide vapors on metal templates have been studied in greater details by Sun et al. [63]. The mechanism follows several complex steps. The initial deposition of the boron oxide vapors leads to the formation of boron oxide nanostructures on the metal surface. Later on, when these nanostructures are heated in the presence of the reducing agents, the oxygen atoms are removed as water vapors, and the nanostructures undergo rearrangement to metastable phases. During this rearrangement, the boron atoms prefer the formation of icosahedral units connected among each other. On the other

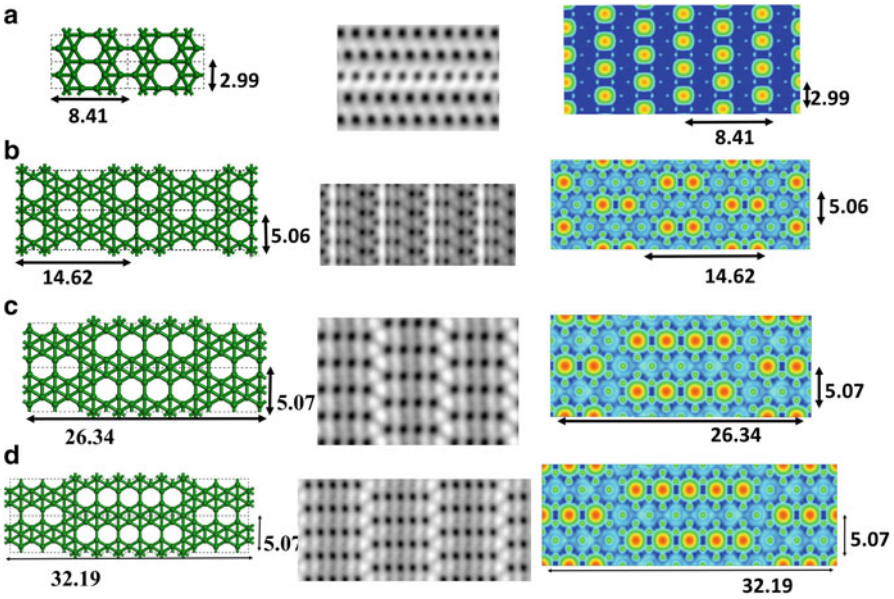

Fig. 2.10 The lattice parameter, simulated STM image, and electron density plots, shown from left to right, for (**a**) χ_3 sheet, (**b**) β_5 sheet, (**c**) β_{32} sheet, and (**d**) β_{33} sheet, respectively. (Reproduced from ref. [51])

hand, the deposition of boron atoms results into formation of monoatomic layers with larger domains. In combination of the theoretical studies and experimental STM images, the most favorable phase is found to have the HD of 1/5; however, the atomic arrangement differs slightly from the χ_3 sheet obtained on Ag(111) surface. The boron layers show corrugation along the perpendicular direction. The unit cell dimensions of the phase is around 21.84 × 15.96 Å, much larger compared to both the β_{12} and χ_3 sheets [13].

A similar scenario is obtained from the molecular dynamics study of the boron clusters and extended boron sheets on Cu(111) surface [58]. The icosahedral clusters disintegrate into planar conformations, but an extended sheet formed of Ih-B_{12} units shows considerable stability and does not undergo any structural transformations. Therefore, the icosahedral sheet is apparently metastable in nature and would rarely disintegrate into planar phases after its formation. However, the formation of the icosahedral sheet would not be possible by boron atom deposition and would need prior control on the experimental conditions.

2.5.3 *Borophene Phases Synthesized on Au Surface*

The Au surface shows differing consequences compared to both the Ag and Cu surfaces because of its inert nature [10]. The Au (111) surface undergoes significant reconstruction, depending upon the surface temperatures, while herringbone reconstruction is observed during the initial stages with lower temperatures, which eventually transform to extended triangular networks with the increase in temperature. Due to the surface reconstruction, the deposition of the boron atoms results into different consequences as well. The lower temperature favors the finite clusters on the surface, whereas upon increasing the temperature, initially the deposited atoms get dissolved with surface Au atoms and diffuse into the bulk Au. Upon cooling to around the room temperature, the boron atoms move to the surface and segregate to smaller rhombohedral islands of boron phases ranging from 0.9 to 1.4 nm^2. Also, the total concentration of boron atoms required for initiating the formation of the monolayers is higher compared to the Ag(111) surface, due to the dissolution of the boron atoms with Au. The inspection of the STM images for the extended borophene phases reveals a periodicity of around 0.66 nm, with slight resemblance with the S1 phase as obtained on Ag(111) surface.

In order to understand the growth mechanism of boron layers on Au surface, DFT computations of the adsorption energetics of boron atoms on the surface were performed. The subsurface near the topmost layer along the step edges was found to offer the more favorable sites than both the surface locations and the bulk interior. In the presence of greater surface strain in Au, the subsurface diffusion of the boron atoms is energetically favored, allowing the formation a stronger Au-B interaction. The smaller boron clusters also favor the subsurface configurations by expelling the surface Au atoms. These clusters would eventually extend to the formation of the larger boron island with more boron atom deposition, removing the surface Au atoms. Figure 2.11 shows the computed energetics for the B diffusion on the surface and subsurface locations.

2.6 Interlayer Stacking of the Borophene Layers

The interlayer stacking possibilities and stabilities of borophene phases show large variations, depending upon the HD and the nonplanar arrangement of the boron atoms [56, 58, 64]. The monolayers could form interlayer bonds varying from trivial two-center covalent bonds to complex multicenter connections or prefer van der Waals interactions. Figures 2.12 and 2.13 shows the most preferred bilayer possibilities of different borophene phases, while in both sheets with zero HD, around half of the boron atoms per unit cell are involved in interlayer B-B bonds (bond density, BD = ½). The planar triangular phase (δ_6 sheet) gets rid of its one excess electron left behind in boron atoms at the hexagonal center upon the formation of the interlayer B-B bond [64, 65]. The bilayer sheet attains a similar

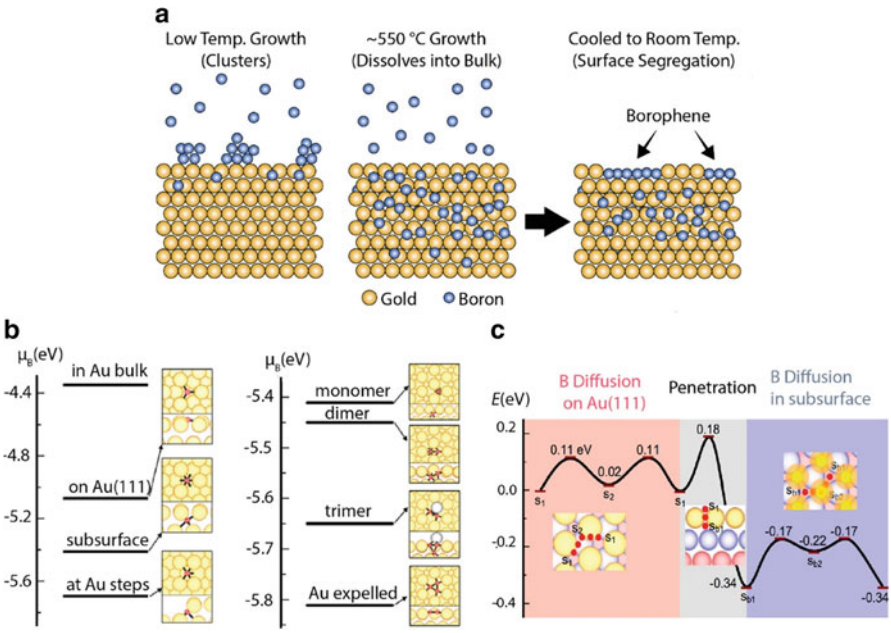

Fig. 2.11 (**a**) The growth mechanism of boron layers on Au surface at three different temperatures [10]. The (**b**) DFT calculations for the energy of boron atoms at different surface and subsurface locations on Au (111) surface and bulk. (**c**) The minimum energy path for the boron atom diffusion on the surface, penetration, and diffusion in subsurface. (Reprinted from ref. [10])

electron count as the AA-stacked graphene bilayer, such that intersection of the *p* bands oriented perpendicular to the hexagonal plane forms two Dirac cones at the Fermi region (Fig. 2.12a–b). With a slight increase in HD to near 1/16, the BD reduces to around ¼ [58]. At further increase of the HD such as in the α-boron bilayer (HD of around 1/9), interlayer B-B bonds are not observed, since the sheet is isoelectronic to graphene. Finally, the graphitic boron sheet (1/3 HD) prefer multicenter B-B bonds between the layers (Fig. 2.13) resembling the three-centered two-electron bonding patterns in several polyhedral boranes and three-dimensional allotropes to satisfy the skeletal electron count.

The relative stability of the bilayer sheets in comparison to the monolayer phases with and without the different metal templates is given in Table 2.2. Without the metal templates, the highest stability is obtained for α_8 sheet with the HD of 1/12, whereas the lowest binding energy is for δ_4 and δ_3 bilayers. On the metal templates, the interlayer interactions are affected by the overlap of the first layer with the metal surface. Most of the bilayers are destabilized compared to the corresponding monolayers on Cu surface. The Ag surface also shows a similar trend. The bilayers formed from the monolayers having higher interaction with the metal surface have lower stability, whereas the reduction in the interaction with the metal surface enhances the stability. However, for the Au surface, both the monolayers with higher

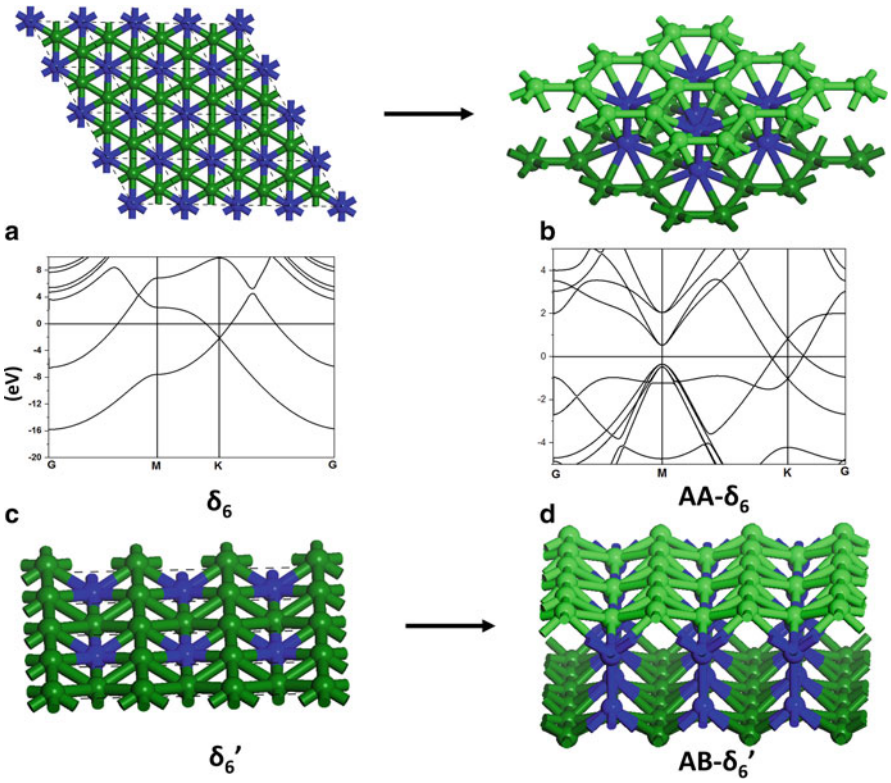

Fig. 2.12 Bilayer structures of boron sheets with zero HD. (**a**) and (**b**) Structure and band structure of monolayer δ_6 and AA-stacked δ_6 sheet. (**c**) δ_6' sheet. (**d**) AB-stacked δ_6' sheet

and lower HD get stabilized. The β_5 and β_{12} bilayers have almost similar stability as the corresponding monolayers, while for δ_6 and α_8 bilayer sheets, the stability is highest.

2.7 The Growth Mechanism of Borophene Phases

Having the thermodynamic data known for the stability of boron phases on different metal surfaces helps in understanding the growth mechanism of boron phases. The formation of 2D boron phases on the metal templates initiates with the formation of 2D boron clusters containing triangular units as the building blocks. Therefore, the nucleation of several 2D metal clusters starting from single boron atoms to around 20 atoms was studied on Cu(111) surface by Liu et al. [66]. The planar clusters containing only triangular B_3 units are found to be the most stable isomers with up to ten boron atoms. The formation of hexagonal hole initiated with the cluster

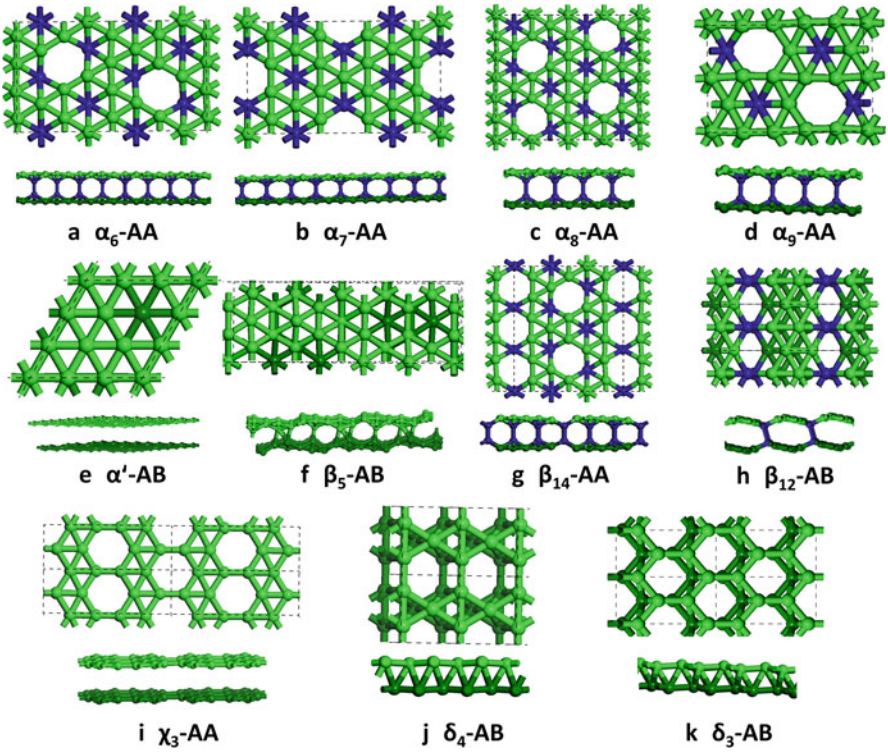

Fig. 2.13 The bilayer stacking possibilities of different monolayer borophenes with varying hole densities, HD. The interlayer bonds are denoted in blue. The bilayer arrangements of the layers are indicated by AA or AB stacking. (Reproduced from ref. [58])

having 11 boron atoms. However, with 12 and more boron atoms, the large number of isomers is obtained with almost similar stability. In most of these clusters, the belt-like elongated isomers containing triangular networks show higher stability. The formation of hexagonal holes is found to be favored, when it is enclosed by a sufficient number of the triangular units surrounding it. The corresponding three-dimensional isomers have lower stability. The 2D clusters undergo slight buckling when adsorbed on the surface, thereby effecting their electronic structures. The in-plane σ-orbitals undergo slight destabilization, whereas the π-orbitals gets lower in energy. The electron density moves from the in-plane molecular orbitals to the π-orbitals centered on the peripheral boron atoms. The energy per boron atom decreases initially with increase in N up to around 12 boron atoms. Beyond that, with the addition of more boron atoms, the formation of energy attains a saturation limit corresponding to the extended boron sheet. Once the metal template has sufficiently large islands of 2D boron clusters, the formation of 2D boron phases continues by joining of these smaller clusters. The molecular dynamics simulations of the boron clusters on the three metal surfaces (Cu, Ag, and Au) provide a similar

Table 2.2 The relative binding energies of boron sheets in meV/atom with respect to α-boron sheet

Sheet	HD	ΔBE_1 (meV/atom)	ΔBE_2 (meV/atom) Cu	Ag	Au	BD
δ_6-AA	**0**	−29	–	69	44	2/6
δ_6'	0	96	50	13	21	
δ_6'-AB	**0**	−109	69	−42	−30	2/8
α_8	1/12 (0.083)	59	–	5	17	
α_8-AA	**1/12 (0.083)**	−146	–	−70	−48	24/88
α	1/9 (0.111)	0	0	0	0	–
β_5	2/15 (0.133)	1	−29	−28	6	–
β_5-AA	**2/15 (0.133)**	−27	63	−12	8	–
β_5-AB	**2/15 (0.133)**	−64	91	−40	15	Multicenter
β_{12}	1/6(0.167)	54	−78	−49	16	–
β_{12}-AA	**1/6(0.167)**	15	112	39	50	–
β_{12}-AB	**1/6(0.167)**	5	92	19	28	2/10

ΔBE_1 denotes the binding energy for the freestanding boron sheets, and ΔBE_2 is the binding energy on metal surfaces. BD denotes bond density, defined as a number of atoms involved in B-B bond formation/total number of atoms per unit cell. The HD of the bilayer borophene sheets are denoted in bold

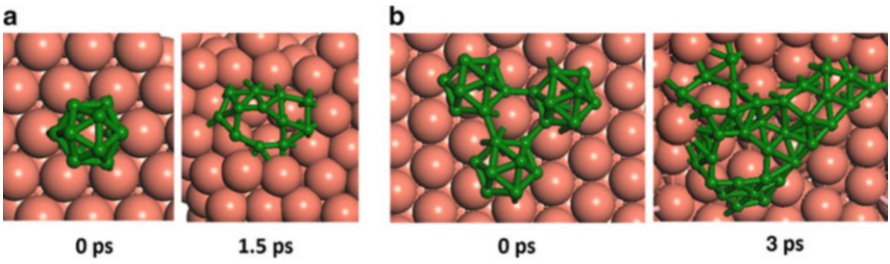

Fig. 2.14 The conformational changes of I_h-boron clusters of different sizes during simulations on Cu(111) surfaces at 1000 K temperature. (Reprinted from ref. [58]). The planar structures are found to be more stable monolayers with the metal surface

overview [58]. When the icosahedral clusters of different sizes are simulated on the metal templates, the rearrangement of the boron atoms to the planar forms is observed. Figure 2.14 shows the structural changes of the boron clusters on Cu(111) surface simulated at 1000 K temperature. For the continuing growth of an established borophene phase, the nanoreactor theory, originally developed for graphene [67], becomes well applicable as was recently demonstrated [68], in good accord with experiments. The formation of bilayers should initiate only after the complete formation of monolayers and depends upon the relative stability and interaction of the monolayers with the metal surface.

2.8 Conclusions and Future Outlook

One can sum up by saying that 2D boron development is a remarkably satisfying, even learning, example in materials science, where decades after semi-intuitive musings on such material possibility, the quantitative structure and synthesis predictions culminated in experimental discoveries. Its notable polymorphism [22, 69] and electronic structure, rich with topological features [55, 70, 71] and promise of superconductivity, motivate the accelerating research. Based upon the first-principles simulations, the most stable 2D boron polymorphs are studied with several future applications in mind. While the presence of hexagonal holes along with the triangular network in the borophene phases are found to enhance the in-plane elasticity and ductility [72], for interconnects in flexible/stretchable electronics, the fluxional multicenter bonding nature provides suitable platform for catalyzing a large number of surface reactions and metal ion mobility [73, 74]. Particularly, the β_{12} sheet with 1/6 HD is theoretically estimated to have a lower diffusion barrier for the Li and Na ions, thereby predicting excellent materials for devising Li and Na ion batteries [74]. Moreover, for several of these polymorphs, the analysis of their phonon spectra and electron-phonon coupling constants reveals superconducting properties with the critical temperature around 10–20 K [55]. Low-damped plasmons sustainable up to visible range [75], along with the unique optical reflectance of borophene layers [76], surpassing in theory even metallic silver, offer applications in reflecting and light-protective coatings.

Though the potential physics and even electronics and plasmonics applications are tantalizing, the challenges remain significant in simplifying the synthetic routes, mostly limited so far to sophisticated beam epitaxy. Separating boron monoatomic layers from the presently all-metal substrates, or finding the ways to grow borophene on insulators-semiconductors, would allow more direct and precise characterization of its intriguing properties, bringing the research to a new level.

References

1. B. Albert, H. Hillebrecht, Boron: Elementary challenge for experimenters and theoreticians. Angew. Chem., Int. Ed **48**, 8640–8668 (2009)
2. E.D. Jemmis, M.M. Balakrishnarajan, Polyhedral boranes and elemental boron: Direct structural relations and diverse electronic requirements. J. Am. Chem. Soc. **123**, 4324–4330 (2001)
3. T. Ogitsu, E. Schwegler, G. Galli, β-Rhombohedral boron: At the crossroads of the chemistry of boron and the physics of frustration. Chem. Rev. **113**, 3425–3449 (2013)
4. A.J. Mannix, X.-F. Zhou, B. Kiraly, J.D. Wood, D. Alducin, B.D. Myers, X. Liu, B.L. Fisher, U. Santiago, J.R. Guest, M.J. Yacaman, A. Ponce, A.R. Oganov, M.C. Hersam, N.P. Guisinger, Synthesis of borophenes: Anisotropic, two-dimensional boron polymorphs. Science **350**, 1513–1516 (2015)
5. B. Feng, J. Zhang, Q. Zhong, W. Li, S. Li, H. Li, P. Cheng, S. Meng, L. Chen, K. Wu, Experimental realization of two-dimensional boron sheets. Nat. Chem. **8**, 563–568 (2016)
6. W.-L. Li, X. Chen, T. Jian, T.-T. Chen, J. Li, L.-S. Wang, From planar boron clusters to borophenes and metalloborophenes. Nat. Rev. Chem. **1**, 0071 (2017)

7. A.P. Sergeeva, I.A. Popov, Z.A. Piazza, W.-L. Li, C. Romanescu, L.-S. Wang, A.I. Boldyrev, Understanding boron through size-selected clusters: Structure, chemical bonding, and fluxionality. Acc. Chem. Res. **47**, 1349–1358 (2014)
8. E.D. Jemmis, D.L. Prasad, Unknowns in the chemistry of boron. Curr. Sci. **95**, 1277–1283 (2008)
9. N. Karmodak, E.D. Jemmis, Fragment approach to the electronic structure of τ-boron allotrope. Phys. Rev. B **95**, 165128 (2017)
10. B. Kiraly, X. Liu, L. Wang, Z. Zhang, A.J. Mannix, B.L. Fisher, B.I. Yakobson, M.C. Hersam, N.P. Guisinger, Borophene synthesis on au(111). ACS Nano **13**, 3816–3822 (2019)
11. Z. Qing, Z. Jin, C. Peng, F. Baojie, L. Wenbin, S. Shaoxiang, L. Hui, M. Sheng, C. Lan, W. Kehui, Metastable phases of 2D boron sheets on Ag(1 1 1). J. Phys.: Condens. Matter **29**, 095002 (2017)
12. G. Tai, T. Hu, Y. Zhou, X. Wang, J. Kong, T. Zeng, Y. You, Q. Wang, Synthesis of atomically thin boron films on copper foils. Angew. Chem., Int. Ed. **54**, 15473–15477 (2015)
13. R. Wu, I.K. Drozdov, S. Eltinge, P. Zahl, S. Ismail-Beigi, I. Božović, A. Gozar, Large-area single-crystal sheets of borophene on cu(111) surfaces. Nat. Nanotechnol. **14**, 44–49 (2019)
14. I. Boustani, Systematic ab initio investigation of bare boron clusters: Determination of the geometry and electronic structures of B_n (n= 2–14). Phys. Rev. B **55**, 16426 (1997)
15. Y. Liu, E.S. Penev, B.I. Yakobson, Probing the synthesis of two-dimensional boron by first-principles computations. Angew. Chem. **125**, 3238–3241 (2013)
16. H. Tang, S. Ismail-Beigi, Novel precursors for boron nanotubes: The competition of two-center and three-center bonding in boron sheets. Phys. Rev. Lett. **99**, 115501 (2007)
17. X. Wu, J. Dai, Y. Zhao, Z. Zhuo, J. Yang, X.C. Zeng, Two-dimensional boron monolayer sheets. ACS Nano **6**, 7443–7453 (2012)
18. X. Yu, L. Li, X.-W. Xu, C.-C. Tang, Prediction of two-dimensional boron sheets by particle swarm optimization algorithm. J. Phys. Chem. C **116**, 20075–20079 (2012)
19. Z. Zhang, Y. Yang, G. Gao, B.I. Yakobson, Two-dimensional boron monolayers mediated by metal substrates. Angew. Chem., Int. Ed. **54**, 13022–13026 (2015)
20. Z. Zhang, S.N. Shirodkar, Y. Yang, B.I. Yakobson, Gate-voltage control of borophene structure formation. Angew. Chem., Int. Ed. **56**, 15421–15426 (2017)
21. S.N. Shirodkar, E.S. Penev, B.I. Yakobson, Honeycomb boron: Alchemy on aluminum pan? Sci. Bull. **63**, 270–271 (2018)
22. E.S. Penev, S. Bhowmick, A. Sadrzadeh, B.I. Yakobson, Polymorphism of two-dimensional boron. Nano Lett. **12**, 2441–2445 (2012)
23. E.D. Jemmis, E.G. Jayasree, Analogies between boron and carbon. Acc. Chem. Res. **36**, 816–824 (2003)
24. I. Boustani, New quasi-planar surfaces of bare boron. Surf. Sci. **370**, 355–363 (1997)
25. I. Boustani, New convex and spherical structures of bare boron clusters. J. Solid State Chem. **133**, 182–189 (1997)
26. H. Hogeveen, P.W. Kwant, J. Postma, P.T. van Duynen, Electronic spectra of pyramidal dications, $(CCH_3)_6^{2+}$ and $(CH)_6^{2+}$. Tetrahedron Lett. **15**, 4351–4354 (1974)
27. E.D. Jemmis, P.V.R. Schleyer, Aromaticity in three dimensions. 4. Influence of orbital compatibility on the geometry and stability of capped annulene rings with six interstitial electrons. J. Am. Chem. Soc **104**, 4781–4788 (1982)
28. M. Böyükata, C. Özdoğan, Z.B. Güvenç, Effects of hydrogen hosting on cage structures of boron clusters: Density functional study of B_mH_n (m = 5–10 and n ≤ m) complexes. Phys. Scr. **77**, 025602 (2008)
29. N. Gonzalez Szwacki, C.J. Tymczak, $B_{12}H_n$ and $B_{12}F_n$: Planar vs icosahedral structures. Nanoscale Res. Lett. **7**, 1–6 (2012)
30. N. Karmodak, R. Chaliha, E.D. Jemmis, Overlap of radial dangling orbitals controls the relative stabilities of polyhedral B_nH_{n-x} isomers (n = 5–12, x = 0 to n – 1). Inorg. Chem. **58**, 3627–3634 (2019)
31. J.K. Olson, A.I. Boldyrev, Planar to 3D transition in the B6Hy anions. J. Phys. Chem. A **117**, 1614–1620 (2013)

32. A.P. Sergeeva, Z.A. Piazza, C. Romanescu, W.-L. Li, A.I. Boldyrev, L.-S. Wang, B_{22}^- and B_{23}^-: All-boron analogues of anthracene and Phenanthrene. J. Am. Chem. Soc. **134**, 18065–18073 (2012)
33. N. Gonzalez Szwacki, A. Sadrzadeh, B.I. Yakobson, B_{80} fullerene: An Ab-initio prediction of geometry, stability, and electronic structure. Phys. Rev. Lett. **98**, 166804 (2007)
34. M.S. Dresselhaus, G. Dresselhaus, P.C. Eklund, *Science of Fullerenes and Carbon Nanotubes: Their Properties and Applications* (Academic press, 1996)
35. E.S. Penev, V.I. Artyukhov, F. Ding, B.I. Yakobson, Unfolding the fullerene: Nanotubes, graphene and poly-elemental varieties by simulations. Adv. Mater. **24**, 4956–4976 (2012)
36. D.L.V.K. Prasad, E.D. Jemmis, Stuffing improves the stability of Fullerenelike boron clusters. Phys. Rev. Lett. **100**, 165504 (2008)
37. D.L.V.K. Prasad, E.D. Jemmis, Stuffed fullerenelike boron carbide nanoclusters. Appl. Phys. Lett. **96**, 023108 (2010)
38. W. Huang, L.-S. Wang, Probing the 2D to 3D structural transition in gold cluster anions using argon tagging. Phys. Rev. Lett. **102**, 153401 (2009)
39. Y. Ohishi, K. Kimura, M. Yamaguchi, N. Uchida, T. Kanayama, Formation of hydrogenated boron clusters in an external quadrupole static attraction ion trap. J. Chem. Phys. **128**, 124304 (2008)
40. Y. Ohishi, K. Kimura, M. Yamaguchi, N. Uchida, T. Kanayama, Synthesis and formation mechanism of hydrogenated boron clusters $B_{12}H_n$ with controlled hydrogen content. J. Chem. Phys. **133**, 074305 (2010)
41. D.Y. Zubarev, A.I. Boldyrev, Comprehensive analysis of chemical bonding in boron clusters. J. Comput. Chem. **28**, 251–268 (2007)
42. D.Y. Zubarev, A.I. Boldyrev, Developing paradigms of chemical bonding: Adaptive natural density partitioning. Phys. Chem. Chem. Phys. **10**, 5207–5217 (2008)
43. B. Kiran, S. Bulusu, H.-J. Zhai, S. Yoo, X.C. Zeng, L.-S. Wang, Planar-to-tubular structural transition in boron clusters: B_{20} as the embryo of single-walled boron nanotubes. Proc. Natl. Acad. Sci. U. S. A. **102**, 961–964 (2005)
44. N. Karmodak, E.D. Jemmis, Exohedral complexation of B_{40}, C_{60} and Arenes with transition metals: A comparative DFT study. Chem. Asian J. **11**, 3350–3354 (2016)
45. H.-J. Zhai, Y.-F. Zhao, W.-L. Li, Q. Chen, H. Bai, H.-S. Hu, Z.A. Piazza, W.-J. Tian, H.-G. Lu, Y.-B. Wu, Y.-W. Mu, G.-F. Wei, Z.-P. Liu, J. Li, S.-D. Li, L.-S. Wang, Observation of an all-boron fullerene. Nat. Chem. **6**, 727–731 (2014)
46. Z.A. Piazza, H.S. Hu, W.L. Li, Y.F. Zhao, J. Li, L.S. Wang, Planar hexagonal B_{36} as a potential basis for extended single-atom layer boron sheets. Nat. Commun. **5**, 3113 (2014)
47. S. Suehara, T. Aizawa, T. Sasaki, Graphenelike surface boron layer: Structural phases on transition-metal diborides (0001). Phys. Rev. B **81**, 085423 (2010)
48. M.E. Jones, R.E. Marsh, The preparation and structure of magnesium boride, MgB_2. J. Am. Chem. Soc. **76**, 1434–1436 (1954)
49. D.L.V.K. Prasad, E.D. Jemmis, Boron and MgB_2 analogs of fullerenes and carbon nanotubes: A density functional theory study. J. Mol. Struc.: THEOCHEM **771**, 111–115 (2006)
50. H. Tang, S. Ismail-Beigi, Self-doping in boron sheets from first principles: A route to structural design of metal boride nanostructures. Phys. Rev. B **80**, 134113 (2009)
51. N. Karmodak, E.D. Jemmis, The role of holes in borophenes: An Ab initio study of their structure and stability with and without metal templates. Angew. Chem., Int. Ed **56**, 10093–10097 (2017)
52. J. Kunstmann, A. Quandt, Broad boron sheets and boron nanotubes: An ab initio study of structural, electronic, and mechanical properties. Phys. Rev. B **74**, 035413 (2006)
53. H. Tang, S. Ismail-Beigi, First-principles study of boron sheets and nanotubes. Phys. Rev. B **82**, 115412 (2010)
54. H. Shu, F. Li, P. Liang, X. Chen, Unveiling the atomic structure and electronic properties of atomically thin boron sheets on an ag(111) surface. Nanoscale **8**, 16284–16291 (2016)
55. E.S. Penev, A. Kutana, B.I. Yakobson, Can two-dimensional boron superconduct? Nano Lett. **16**, 2522–2526 (2016)

56. N. Gao, X. Wu, X. Jiang, Y. Bai, J. Zhao, Structure and stability of bilayer borophene: The roles of hexagonal holes and interlayer bonding. FlatChem **7**, 48–54 (2018)
57. L.Z. Zhang, Q.B. Yan, S.X. Du, G. Su, H.J. Gao, Boron sheet adsorbed on metal surfaces: Structures and electronic properties. J. Phys. Chem. C **116**, 18202–18206 (2012)
58. N. Karmodak, E.D. Jemmis, Metal templates and boron sources controlling Borophene structures: An ab initio study. J. Phys. Chem. C **122**, 2268–2274 (2018)
59. Z. Zhang, A.J. Mannix, Z. Hu, B. Kiraly, N.P. Guisinger, M.C. Hersam, B.I. Yakobson, Substrate-induced nanoscale undulations of Borophene on silver. Nano Lett. **16**, 6622–6627 (2016)
60. X. Liu, Z. Zhang, L. Wang, B.I. Yakobson, M.C. Hersam, Intermixing and periodic self-assembly of borophene line defects. Nat. Mater. **17**, 783–788 (2018)
61. W. Li, L. Kong, C. Chen, J. Gou, S. Sheng, W. Zhang, H. Li, L. Chen, P. Cheng, K. Wu, Experimental realization of honeycomb borophene. Sci. Bull. **63**, 282–286 (2018)
62. X. Liu, L. Wang, S. Li, M.S. Rahn, B.I. Yakobson, M.C. Hersam, Geometric imaging of borophene polymorphs with functionalized probes. Nat. Commun. **10**, 1642 (2019)
63. X. Sun, X. Liu, J. Yin, J. Yu, Y. Li, Y. Hang, X. Zhou, M. Yu, J. Li, G. Tai, W. Guo, Two-dimensional boron crystals: Structural stability, tunable properties, fabrications and applications. Adv. Funct. Mater. **27**, 1603300 (2017)
64. F. Ma, Y. Jiao, G. Gao, Y. Gu, A. Bilic, Z. Chen, A. Du, Graphene-like two-dimensional ionic boron with double Dirac cones at ambient condition. Nano Lett. **16**, 3022–3028 (2016)
65. X.-F. Zhou, X. Dong, A.R. Oganov, Q. Zhu, Y. Tian, H.-T. Wang, Semimetallic two-dimensional boron allotrope with massless Dirac fermions. Phys. Rev. Lett. **112**, 085502 (2014)
66. H. Liu, J. Gao, J. Zhao, From boron cluster to two-dimensional boron sheet on cu(111) surface: Growth mechanism and hole formation. Sci. Rep. **3**, 3238 (2013)
67. V.I. Artyukhov, Y. Liu, B.I. Yakobson, Equilibrium at the edge and atomistic mechanisms of graphene growth. Proc. Natl. Acad. Sci. **109**, 15136–15140 (2012)
68. Z. Zhang, A.J. Mannix, X. Liu, Z. Hu, N.P. Guisinger, M.C. Hersam, B.I. Yakobson, Near-equilibrium growth from borophene edges on silver. Sci. Adv **5**, eaax0246 (2019)
69. Z. Zhang, E.S. Penev, B.I. Yakobson, Two-dimensional materials: Polyphony in B flat. Nat. Chem. **8**, 525–527 (2016)
70. B. Feng, O. Sugino, R.-Y. Liu, J. Zhang, R. Yukawa, M. Kawamura, T. Iimori, H. Kim, Y. Hasegawa, H. Li, L. Chen, K. Wu, H. Kumigashira, F. Komori, T.-C. Chiang, S. Meng, I. Matsuda, Dirac fermions in Borophene. Phys. Rev. Lett. **118**, 096401 (2017)
71. H. Zhang, Y. Xie, Z. Zhang, C. Zhong, Y. Li, Z. Chen, Y. Chen, Dirac nodal lines and tilted semi-Dirac cones coexisting in a striped boron sheet. J. Phys. Chem. Lett. **8**, 1707–1713 (2017)
72. Z. Zhang, Y. Yang, E.S. Penev, B.I. Yakobson, Elasticity, flexibility, and ideal strength of Borophenes. Adv. Funct. Mater. **27**, 1605059 (2017)
73. C. Liu, Z. Dai, J. Zhang, Y. Jin, D. Li, C. Sun, Two-dimensional boron sheets as metal-free catalysts for hydrogen evolution reaction. J. Phys. Chem. C **122**, 19051–19055 (2018)
74. X. Zhang, J. Hu, Y. Cheng, H.Y. Yang, Y. Yao, S.A. Yang, Borophene as an extremely high capacity electrode material for Li-ion and Na-ion batteries. Nanoscale **8**, 15340–15347 (2016)
75. Y. Huang, S.N. Shirodkar, B.I. Yakobson, Two-dimensional boron polymorphs for visible range Plasmonics: A first-principles exploration. J. Am. Chem. Soc. **139**, 17181–17185 (2017)
76. S. Gupta, S.N. Shirodkar, A. Kutana, B.I. Yakobson, In pursuit of 2D materials for maximum optical response. ACS Nano **12**, 10880–10889 (2018)